

# RSC Advances



This is an *Accepted Manuscript*, which has been through the Royal Society of Chemistry peer review process and has been accepted for publication.

*Accepted Manuscripts* are published online shortly after acceptance, before technical editing, formatting and proof reading. Using this free service, authors can make their results available to the community, in citable form, before we publish the edited article. This *Accepted Manuscript* will be replaced by the edited, formatted and paginated article as soon as this is available.

You can find more information about *Accepted Manuscripts* in the [Information for Authors](#).

Please note that technical editing may introduce minor changes to the text and/or graphics, which may alter content. The journal's standard [Terms & Conditions](#) and the [Ethical guidelines](#) still apply. In no event shall the Royal Society of Chemistry be held responsible for any errors or omissions in this *Accepted Manuscript* or any consequences arising from the use of any information it contains.

# Investigation of luminescence properties and energy transfer mechanism of $\text{Li}_6\text{Lu}(\text{BO}_3)_3:\text{Ce}^{3+},\text{Tb}^{3+}$ green-emitting phosphors

Cite this: *RSC Advance*, 2014, xx, xx

Irish Valerie B. Maggay, Pin-Chun Lin and Wei-Ren Liu\*

$\text{Li}_6\text{Lu}(\text{BO}_3)_3:\text{Ce}^{3+},\text{Tb}^{3+}$  phosphor was synthesized via a conventional solid-state method. The phase purity, photoluminescence properties, energy transfer mechanism, thermal stability and chromaticity coordinates were investigated. The absorption spectrum was comprised of broad bands in the UV region and the emission spectrum was consisted of characteristic peaks from both  $\text{Ce}^{3+}$  and  $\text{Tb}^{3+}$  under UV excitation. The amount of  $\text{Ce}^{3+}$  was fixed to 3 mol % while  $\text{Tb}^{3+}$  was varied from 20 to 80 mol % and the chromaticity coordinates were tuned from blue to green region. The energy transfer mechanism between  $\text{Ce}^{3+}$  and  $\text{Tb}^{3+}$  was attributed to quadrupole-quadrupole interaction and the critical distance was measured to be 8.12 Å. The overall performance of the phosphor was enhanced by the efficient energy transfer between  $\text{Ce}^{3+}$  and  $\text{Tb}^{3+}$  ions.

Received 00th xx 2014,  
Accepted 00th xx 2014

htDOI: 10.1039/x0xx00000x

[www.rsc.org/dalton](http://www.rsc.org/dalton)

## Introduction

White light emitting diodes (W-LEDs) have provided remarkable advances in lighting technologies and displays. They have gained significant attention over conventional lighting sources due to its advantages such as low energy consumption, long operational lifetime, high efficiency, high stability and less environmental threat [1-11]. Commercially available W-LEDs are fabricated by combining blue emitting InGaN-based LED chip covered by yellow emitting phosphor  $\text{Y}_3\text{Al}_5\text{O}_{12}:\text{Ce}^{3+}$  (YAG) [1,2,4,6,7,10,11]. However, YAG suffers from inevitable drawbacks such as low color rendering index (CRI) ( $\text{Ra}<80$ ) and high correlated color temperature (CCT) ( $T_c>4500\text{K}$ ) due to the insufficient red emission in the visible spectrum [1-4,6-8,10-11]. Moreover, blue LED chip and yellow phosphor have different degradation rates causing chromatic aberration and decreased efficiency over long period of time [1]. To overcome these defects, a new method has been developed by coupling red, green and blue tricolor phosphors with n-UV LED chip in order to produce high CRI, high color stability and good color uniformity [1,2,6,7,10]. Thus, developments of new phosphors with high chemical stability and strong absorption in UV or near-UV region with high conversion efficiency are highly crucial [1-3,10].

Borate compounds are widely used in nonlinear optics, piezo and scintillation techniques and phosphors for W-LEDs [12] due to its low synthesizing temperature and high physical and chemical stability [2]. Recent investigations were conducted on  $\text{NaSrBO}_3:\text{Ce}^{3+}$  [2],  $\text{MSr}_4(\text{BO}_3)_3:\text{Ce}^{3+}$  ( $\text{M} = \text{Li}$  and  $\text{Na}$ ) [3],  $\text{Ca}_3\text{Y}_2(\text{BO}_3)_4:\text{Eu}^{3+}$  [4],  $\text{Na}_3\text{La}_2(\text{BO}_3)_3:\text{Ce}^{3+},\text{Tb}^{3+}$  [5],  $\text{KSr}_4(\text{BO}_3)_3:\text{Eu}^{3+}$  [7],  $\text{LiSr}_4(\text{BO}_3)_3:\text{Ce}^{3+},\text{Eu}^{2+}$  [11],  $\text{LiCaBO}_3$  [13],  $\text{Ba}_2\text{Ca}(\text{BO}_3)_2:\text{Ce}^{3+}$  [14] and  $\text{KCa}_4(\text{BO}_3)_3:\text{Ln}^{3+}$  ( $\text{Ln} = \text{Dy}, \text{Eu}, \text{Tb}$ ) [15]. ( $\text{Li}_6\text{Ln}(\text{BO}_3)_3$  ( $\text{Ln} = \text{Gd}, \text{Y}$ ) were investigated and showed promising results on W-LEDs and nonlinear optics application [12,17-19].  $\text{Li}_6\text{Lu}(\text{BO}_3)_3$  host was first synthesized and studied by Yang et al. [16] and Fuwad et al. [20] and it exhibited potential applications for neutron detection scintillator).

Energy transfer plays a crucial role in enhancing the luminescent properties of rare earth ions such as  $\text{Tb}^{3+}$  and  $\text{Eu}^{3+}$  which display only narrow excitation peaks near UV region due to the forbidden f-f transition and only yield sharp and weak emission peaks [1].  $\text{Ce}^{3+}$  is not only used as an activator but also as a sensitizer. It can generate strong excitation peaks near UV region and can provide efficient conversion to longer wavelengths [22]. Several  $\text{Ce}^{3+}$  and  $\text{Tb}^{3+}$  co-doped phosphors were synthesized such as  $\text{Ba}_3\text{Gd}(\text{PO}_4)_3:\text{Ce}^{3+},\text{Tb}^{3+}$  [1],  $\text{Na}_3\text{La}_2(\text{BO}_3)_3:\text{Ce}^{3+},\text{Tb}^{3+}$  [5],  $\text{SrMgSi}_2\text{O}_6:\text{Ce},\text{Tb}$  [6],  $\text{Sr}_2\text{B}_3\text{O}_9\text{Cl}:\text{Ce}^{3+},\text{Tb}^{3+}$  [8],

$\text{BaAl}_2\text{B}_2\text{O}_7:\text{Ce}^{3+},\text{Tb}^{3+}$  [9],  $\text{Sr}_3\text{MgSi}_2\text{O}_8:\text{Ce}^{3+},\text{Tb}^{3+}$  [10],  $\text{SrAl}_2\text{B}_2\text{O}_7:\text{Ce}^{3+},\text{Tb}^{3+}$  [21],  $\text{Ca}_3\text{Y}_2\text{Si}_3\text{O}_{12}:\text{Ce}^{3+},\text{Tb}^{3+}$  [23] and so on.

To the best of our knowledge, the luminescence properties of  $\text{Li}_6\text{Lu}(\text{BO}_3)_3:\text{Ce}^{3+},\text{Tb}^{3+}$  have not been investigated yet. As we know, borate host has lower synthesizing temperature than that of other host phosphors, such as silicon-based, aluminum-based and nitride-based system. These borated-based phosphors, such as  $\text{Sr}_2\text{B}_2\text{O}_5:\text{Ce}^{3+},\text{Tb}^{3+}$  (1073 K),  $\text{NaCaBO}_3$  (1123 K),  $\text{KCa}_4(\text{BO}_3)_3$  (1073 K) have been reported [2, 15, 26, 27]. In this study, pure phased- $\text{Li}_6\text{Lu}(\text{BO}_3)_3$  was obtained at a much lower temperature of 973 K with high purity, which give advantages of energy-saving and cost-effective. In this study, the crystal structure, photoluminescence (PL) properties, color chromaticity, energy transfer mechanism between the sensitizer and activator, and thermal quenching were investigated. The results indicate that  $\text{Li}_6\text{Lu}(\text{BO}_3)_3:\text{Ce}^{3+},\text{Tb}^{3+}$  is a potential green emitting phosphor for UV-LED applications.

## Experimental section

### Materials and synthesis

A series of rare earth-doped  $\text{Li}_6\text{Lu}(\text{BO}_3)_3:x\text{Ce}^{3+},y\text{Tb}^{3+}$  ( $x = 0.005, 0.01, 0.03, 0.05, 0.07, 0.10$  mol and  $y = 0.20, 0.40, 0.60, 0.70$  and  $0.80$  mol) phosphors were synthesized via solid state reactions. The reactants used were  $\text{Li}_2\text{CO}_3$  (99.99%, Aldrich),  $\text{H}_3\text{BO}_3$  (99.99%, Aldrich),  $\text{Lu}_2\text{O}_3$  (99.99, Aldrich),  $\text{CeO}_2$  (99.99%, Aldrich) and  $\text{Tb}_4\text{O}_7$  (99.99%, Aldrich). The stoichiometric proportions of the precursors were weighed and thoroughly ground in an agate mortar. Subsequently, the powder was heated at 973 K for 8 hours under a reducing atmosphere (15%  $\text{H}_2/85\%$   $\text{N}_2$ ). The products were then cooled down to ambient temperature and ground for further analyses.

### Materials characterization

The crystallinity of the as-synthesized samples were characterized using X-ray diffractometer with  $\text{Cu K}\alpha$  ( $\lambda=1.5418$  Å) generated at 45 KV and 30 mA. Data were gathered in the  $2\theta$  range of  $10^\circ$  to  $80^\circ$  with a scan speed of  $5^\circ/\text{min}$ . The luminescence properties of the samples were determined using PL/PLE at room temperature and were recorded by a Spex-Fluorolog-3 spectrophotometer equipped with 450 W Xenon light source and measured with a scan rate of  $150$  nm  $\text{min}^{-1}$ . Commission International de l'Eclairage (CIE) chromaticity coordinates of the samples were measured using a Laiko DT-101 color analyzer equipped with a CCD detector (Laiko Co., Tokyo, Japan).

## Results and discussion

### XRD and crystal structure investigation

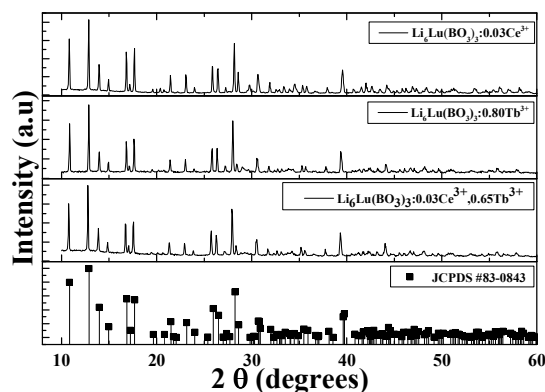


Figure 1. XRD patterns of different samples synthesized at 973 K for 8 hours under 15%  $\text{H}_2/85\%$   $\text{N}_2$  reducing atmosphere.

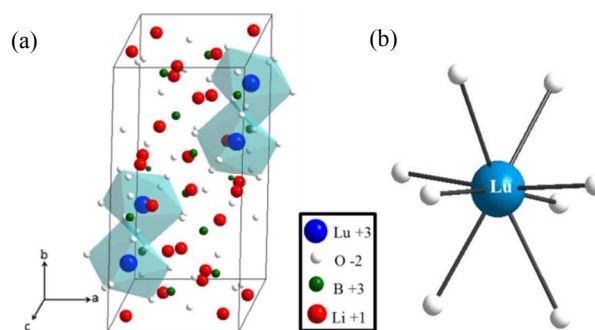


Figure 2. (a) Crystal structure of  $\text{Li}_6\text{Lu}(\text{BO}_3)_3$  and (b) coordination environment of  $\text{Lu}^{3+}$  ion.

The X-ray powder diffraction (XRD) patterns of  $\text{Li}_6\text{Lu}(\text{BO}_3)_3$  doped with  $0.03$   $\text{Ce}^{3+}$ ,  $0.80$   $\text{Tb}^{3+}$  and  $0.03$   $\text{Ce}^{3+}$ ,  $0.65$   $\text{Tb}^{3+}$  are presented in Figure 1. The data indicate that the peaks of the samples were consistent with the standard JCPDS #83-0843 and no impurities were observed even with heavy doping of  $\text{Tb}^{3+}$  ions. Therefore, pure-phased samples were obtained.  $\text{Lu}^{3+}$  ions were successfully substituted by  $\text{Ce}^{3+}$  ions and  $\text{Tb}^{3+}$  ions due to their comparable ionic radii ( $\text{Lu}^{3+} = 0.977$  Å,  $\text{Ce}^{3+} = 1.14$  Å,  $\text{Tb}^{3+} = 1.04$  Å).  $\text{Li}_6\text{Lu}(\text{BO}_3)_3$  host phosphor belongs to the monoclinic system of  $\text{Li}_6\text{RE}(\text{BO}_3)_3$  ( $\text{RE} = \text{Gd}, \text{Y}, \text{Yb}, \text{Ho}$ ) and space group of  $\text{P}_{21/c}$  [12,16,17]. The lattice parameters were calculated to be  $a = 0.7236$  nm,  $b = 1.6584$  nm,  $c = 0.6693$  nm and  $\beta = 105.42^\circ$ . The crystal structure of  $\text{Li}_6\text{Lu}(\text{BO}_3)_3$  is shown in Figure 2(a). The structural unit of  $\text{Li}_6\text{Ln}(\text{BO}_3)_3$  ( $\text{Ln} = \text{Gd}, \text{Y}, \text{Lu}$ ) consists of isolated boron with a triangular coordination with oxygen atoms,  $\text{Li}^+$  ions are surrounded by four or five oxygen atoms forming trigonal bipyramids or tetrahedron prisms, and distorted eight-fold  $\text{Lu}^{3+}$  with  $\text{C}_1$  site symmetry.  $\text{LuO}_8$  polyhedra are connected with each other by common edges along the direction oblique to the  $c$  axis [9, 12, 18].

### Photoluminescence properties of $\text{Li}_6\text{Lu}(\text{BO}_3)_3:x\text{Ce}^{3+}$

Figure 3 illustrates the PL/PLE of  $\text{Li}_6\text{Lu}(\text{BO}_3)_3:x\text{Ce}^{3+}$ . When the sample is excited at 350 nm it displays an asymmetric broad band from 360-480 nm. This phenomenon was due to the dual emission of  $\text{Ce}^{3+}$  attributed to the parity allowed transition from the

lowest 5d level to the  ${}^2F_{5/2}$  and  ${}^2F_{7/2}$  ascribed to the spin-orbit coupling of the 4f ground state of  $\text{Ce}^{3+}$  [6,9,10,23]. The emission band can be decomposed into two Gaussian profiles with maximum peaks at approximately 382 nm ( $26,178\text{ cm}^{-1}$ ) and 415 nm ( $24,096\text{ cm}^{-1}$ ) depicted in the inset with a difference of approximately  $2,082\text{ cm}^{-1}$ . This result is comparable to the theoretical value of  $\approx 2,000\text{ cm}^{-1}$  [2,10,11]. The excitation spectrum monitored at 400 nm consists of two broad bands with maximum peak at 350 nm which was due to the  $4f \rightarrow 5d$  transition of  $\text{Ce}^{3+}$  [1,2,6,8,9,21].

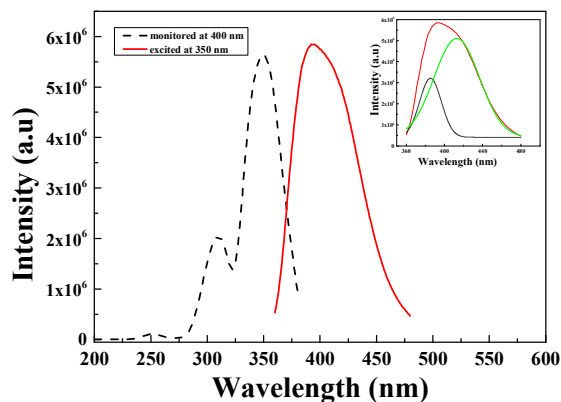


Figure 3. PL/PLE of  $\text{Li}_6\text{Lu}_{0.97}(\text{BO}_3)_3:0.03\text{Ce}^{3+}$  excited at 350 nm and monitored at 400 nm. Inset shows the Gaussian deconvolution of  $\text{Ce}^{3+}$  emission.

A series of 0.005, 0.01, 0.03, 0.05, 0.07 and 0.10 mol concentration of  $\text{Ce}^{3+}$  were prepared and is presented in Figure 4. It is evident that the emission intensity of samples initially increases as the  $\text{Ce}^{3+}$  increases until reaches maximum intensity at 3 mol %. Further increase of  $\text{Ce}^{3+}$  concentration resulted in decreased intensity due to the concentration quenching of the  $\text{Ce}^{3+}$ . Also, it is noticeable that the emission spectra are shifted to a longer wavelength at higher  $\text{Ce}^{3+}$  concentration and the peak emission is red shifted from 388 nm to 398 nm which is attributed to the increase of crystal field effect [8].

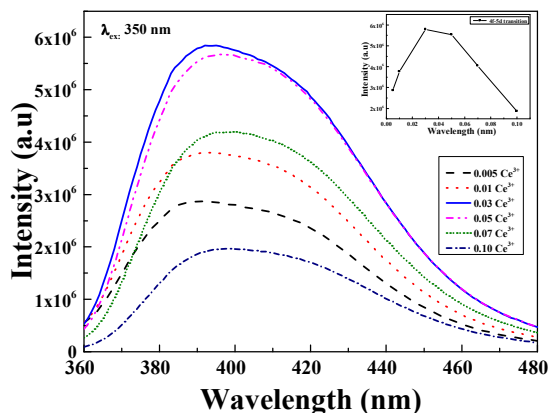


Figure 4. PL of  $\text{Li}_6\text{Lu}_{1-x}(\text{BO}_3)_3:x\text{Ce}^{3+}$  ( $x = 0.5, 1, 3, 5, 7$  and  $10\text{ mol}\%$ ) excited at 350 nm. Inset: PL intensity of  $\text{Li}_6\text{Lu}(\text{BO}_3)_3:\text{Ce}^{3+}$  as a function of  $\text{Ce}^{3+}$  concentration.

### Photoluminescence properties of $\text{Li}_6\text{Lu}_{1-y}(\text{BO}_3)_3:y\text{Tb}^{3+}$

The ground state for  $\text{Tb}^{3+}$  ions with  $4f^8$  configuration is  ${}^7F^1$ . When  $\text{Tb}^{3+}$  is excited it is promoted to the 5d shell which generates two  $4f^75d^1$  excitation states, a high spin state with  ${}^9D_J$  configurations or a low spin state with  ${}^7D_J$  configurations. According to Hund's rule,  ${}^9D_J$  levels have lower energy as a result; the transitions from  ${}^7F_J \rightarrow {}^9D_J$  are spin-forbidden while  ${}^7F_J \rightarrow {}^7D_J$  transitions are spin-allowed [23]. Figure 5 shows the PL/PLE of  $\text{Li}_6\text{Lu}_{1-y}(\text{BO}_3)_3:y\text{Tb}^{3+}$ . The absorption spectrum monitored at 543 nm is comprised of narrow peaks from 200-275 nm attributed to the spin allowed  $4f^8 \rightarrow 4f^75d^1$  transition and sharp peaks from 300-400 nm located at 281, 303, 319, 342, 354, 360 and 377 nm are due to the forbidden 4f-4f transitions of  $\text{Tb}^{3+}$  ions from  ${}^7F_6$ , to  ${}^5I_7$ ,  ${}^5H_7$ ,  ${}^5D_{0,1}$ ,  ${}^5G_{2,3,4}$ ,  ${}^5D_2$ ,  ${}^5L_{10}$ , and  ${}^5D_3$  levels, respectively [8]. The highest peak is centered at 377 nm indicating that the phosphor can be efficiently excited by n-UV chips.  $\text{Tb}^{3+}$  can be an activator for blue and green phosphors. At lower concentration, it emits blue color on the other hand, at higher concentrations, it exhibits green emission. When the sample is excited at 377 nm, the emission spectrum exhibits four sharp peaks located at 489 nm, 543 nm, 591 nm and 618 nm which are assigned to the  ${}^5D_4 \rightarrow {}^7F_J$  ( $J = 6, 5, 4$  and  $3$ ) ascribed to the characteristic transition of  $\text{Tb}^{3+}$ , respectively. The phosphor exhibits green emitting hue due to the maximum peak at 543 nm corresponding to  ${}^5D_4 \rightarrow {}^7F_5$  transition that is due to magnetic dipole transition.

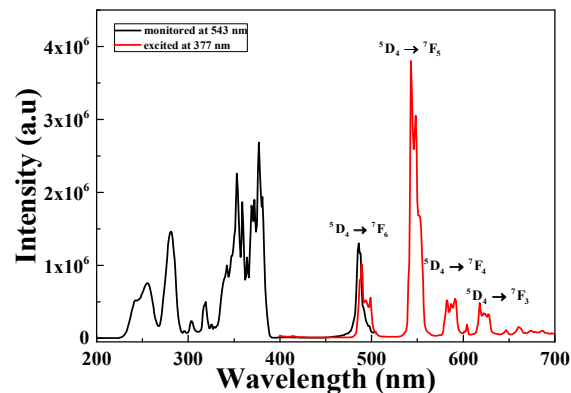


Figure 5. PL/PLE of  $\text{Li}_6\text{Lu}_{0.40}(\text{BO}_3)_3:0.60\text{Tb}^{3+}$  excited at 377 nm and monitored at 543 nm

Different concentrations of  $\text{Li}_6\text{Lu}_{1-y}(\text{BO}_3)_3:y\text{Tb}^{3+}$  ( $y = 0.20-0.80\text{ mol}$ ) were synthesized and its corresponding emission intensities are illustrated in Figure 6. The luminescence intensity of samples increased gradually as the concentration of  $\text{Tb}^{3+}$  ions increased. It reached maximum intensity at 60 mol % and began to decrease. This phenomenon is a result of the concentration quenching of the  $\text{Tb}^{3+}$  ions.  ${}^5D_3 \rightarrow {}^5D_4$  is resonant with  ${}^7F_6 \rightarrow {}^7F_0$  transition therefore, the emission due to  ${}^5D_3 \rightarrow {}^7F_J$  transitions are often quenched at high  $\text{Tb}^{3+}$  content because of the cross relaxation  ${}^5D_3 + {}^7F_6 \rightarrow {}^5D_4 + {}^7F_0$  [1,9]. The concentration quenching is higher than most  $\text{Tb}^{3+}$  doped phosphors. A possible reason is linked to the structure of  $\text{Li}_6\text{Lu}(\text{BO}_3)_3$  which the zigzag structure of the activator ion restrict the energy migration to one dimension. Therefore, the

probability of the migrating excitation to encounter the randomly distributed killer site is lessened [10,12,17].

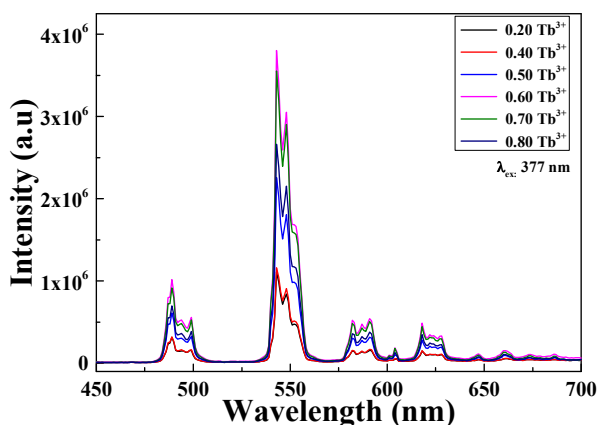


Figure 6. PL of  $\text{Li}_6\text{Lu}_{1-y}(\text{BO}_3)_3:y\text{Tb}^{3+}$  ( $y = 20, 40, 50, 60, 70,$  and  $80$  mol%) excited at  $377$  nm.

### Photoluminescence properties of $\text{Li}_6\text{Lu}_{0.97-y}(\text{BO}_3)_3:0.03\text{Ce}^{3+},y\text{Tb}^{3+}$

The  $5d-4f$  transition of  $\text{Ce}^{3+}$  is electric dipole allowed and is evidently stronger compared to the  $4f-4f$  intra-configurational transition of  $\text{Tb}^{3+}$ . Figures 7 (a), (b) and (c) depict the PL/PLE comparison of singly doped  $\text{Ce}^{3+}$ ,  $\text{Tb}^{3+}$  and  $\text{Ce}^{3+}\text{-Tb}^{3+}$  co-doped  $\text{Li}_6\text{Lu}(\text{BO}_3)_3$  phosphor. It is evident that there is a spectral overlap between the emission spectrum of  $\text{Ce}^{3+}$  in Figure 7a and excitation spectrum of  $\text{Tb}^{3+}$  in Figure 7b which implies that energy transfer between  $\text{Ce}^{3+}$  and  $\text{Tb}^{3+}$  is expected in  $\text{Li}_6\text{Lu}(\text{BO}_3)_3$  host. In Figure 7c, there is an obvious overlap between the emission and excitation spectra of  $\text{Ce}^{3+}\text{-Tb}^{3+}$  co-doping that verifies that the energy absorbed by  $\text{Ce}^{3+}$  is efficiently transferred to  $\text{Tb}^{3+}$  thus;  $\text{Ce}^{3+}$  is an efficient sensitizer for  $\text{Tb}^{3+}$ . Furthermore, there is a broad absorption band at UV region attributed to  $\text{Ce}^{3+}$  which makes it suitable to be excited by n-UV LED chip.

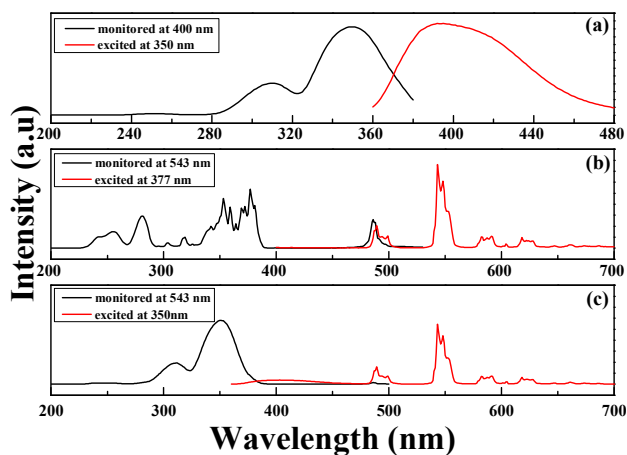


Figure 7 (a). PL/PLE of  $\text{Li}_6\text{Lu}(\text{BO}_3)_3:0.01\text{Ce}^{3+}$  excited at  $350$  nm and monitored at  $400$  nm; (b) PL/PLE of  $\text{Li}_6\text{Lu}(\text{BO}_3)_3:0.60\text{Tb}^{3+}$  excited at  $377$  nm and monitored at  $543$  nm; (c) PL/PLE of

$\text{Li}_6\text{Lu}(\text{BO}_3)_3:0.03\text{Ce}^{3+},0.65\text{Tb}^{3+}$  excited at  $350$  nm and monitored at  $543$  nm.

Energy transfer between sensitizer and activator enhances the emission intensity. Figure 8 illustrates the investigation of series of phosphors co-doped with  $3$  mol % of  $\text{Ce}^{3+}$  and varying concentrations of  $\text{Tb}^{3+}$  ( $y = 20-80$  mol %) excited at  $350$  nm. The broad band situated from  $360-450$  nm is ascribed to the  $5d-4f$  transition of  $\text{Ce}^{3+}$  ions while the narrow peaks  $475-650$  nm are assigned to the  ${}^5\text{D}_4 \rightarrow {}^7\text{F}_J$  ( $J = 6,5,4$  and  $3$ ) transitions of  $\text{Tb}^{3+}$  with maximum peak at  $543$  nm emitting a green color. The PL intensity initially increases as the concentration of  $\text{Tb}^{3+}$  increases until it reached its optimum concentration at  $x = 0.03, y = 0.65$ . As the  $\text{Tb}^{3+}$  concentration further increases, the emission intensity decreases as a result of concentration quenching. Conversely, the intensity of  $\text{Ce}^{3+}$  is inversely proportional to the concentration of  $\text{Tb}^{3+}$ . These results denote that an effective energy transfer occurred. Moreover, comparing the PL of Figure 8 with Figure 6, it is highly evident that the intensity of  $\text{Ce}^{3+}\text{-Tb}^{3+}$  co-doping is higher than singly doped  $\text{Tb}^{3+}$  proving that  $\text{Ce}^{3+}$  is an efficient sensitizer.

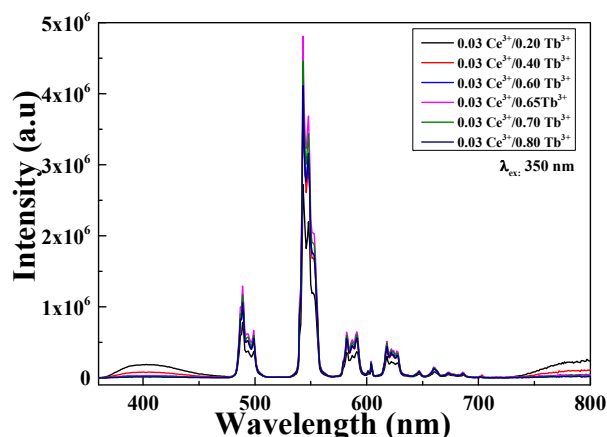


Figure 8. PL of  $\text{Li}_6\text{Lu}(\text{BO}_3)_3:0.03\text{Ce}^{3+},y\text{Tb}^{3+}$  ( $y = 20, 40, 60, 65,$  and  $80$  mol%) excited at  $350$  nm and monitored at  $543$  nm.

### Schematic diagram of Energy Transfer

The energy levels and energy transfer mechanism are illustrated in the schematic diagram in Figure 9. When excited at  $350$  nm,  $\text{Ce}^{3+}$  ions are excited to the  $5d$  configuration then the ions relax non-radiatively to the lowest of  $5d$  state. The excited ions return to its ground state at  ${}^2\text{F}_{5/2}$  and  ${}^2\text{F}_{7/2}$  levels with a consequent broad band emission. As a consequence of the matched energy levels of  $\text{Ce}^{3+}$  and  $\text{Tb}^{3+}$ , the sensitizer ( $\text{Ce}^{3+}$ ) can transfer its energy to the activator ( $\text{Tb}^{3+}$ ) thence causing  $\text{Tb}^{3+}$  ions to excite from its ground state.  $\text{Tb}^{3+}$  ions relax at level  ${}^5\text{D}_3$  with subsequent  ${}^5\text{D}_3 \rightarrow {}^7\text{F}_J$  transitions. Cross-relaxation might occur between  ${}^5\text{D}_3$  and  ${}^5\text{D}_4$  simultaneously with increasing amount of  $\text{Tb}^{3+}$  generating stronger emissions and higher intensities at  ${}^5\text{D}_4 \rightarrow {}^7\text{F}_J$  transitions while leading to a decrease in  ${}^5\text{D}_3$  emission. Finally, the excited  $\text{Tb}^{3+}$  ions return to its ground state with a subsequent emission of green luminescence [1,6].

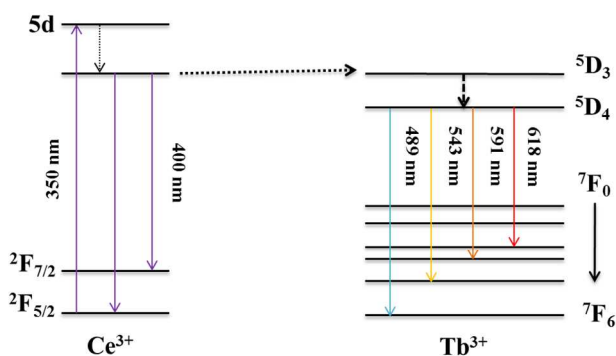


Figure 9. The schematic energy levels of  $\text{Ce}^{3+}$  and  $\text{Tb}^{3+}$  with energy transfer mechanism.

### $\text{Ce}^{3+} \rightarrow \text{Tb}^{3+}$ Energy Transfer

In order to further analyze the energy transfer between  $\text{Ce}^{3+}$  and  $\text{Tb}^{3+}$ , Figure 10 presents the energy transfer efficiency of  $\text{Ce}^{3+}$  and  $\text{Tb}^{3+}$ , 4f-5d transition of  $\text{Ce}^{3+}$  and  $^5\text{D}_4 \rightarrow ^7\text{F}_5$  transition of  $\text{Tb}^{3+}$  all as a function of  $\text{Tb}^{3+}$  concentration in  $\text{Li}_6\text{Lu}(\text{BO}_3)_3$  phosphor excited at 350 nm. The energy transfer efficiency ( $\eta_{ET}$ ) can be calculated using following equation [1,6,8-9]:

$$\eta_T = 1 - \frac{I_S}{I_{SO}} \quad (1)$$

where  $I_S$  and  $I_{SO}$  are the luminescence intensities of  $\text{Ce}^{3+}$  in the presence and absence of  $\text{Tb}^{3+}$ , respectively. The value of  $\eta_{ET}$  increases gradually with an increase of  $\text{Tb}^{3+}$  concentration. When  $\text{Tb}^{3+}$  concentration increased to 65 mol %, the  $\eta_T$  increased to 99.60 % indicating efficient energy transfer between the sensitizer and activator. The intensities of 4f-5d transition of  $\text{Ce}^{3+}$  decreased as the amount of  $\text{Tb}^{3+}$  increased thus the energy of  $\text{Ce}^{3+}$  ions is successfully transferred to its neighboring  $\text{Tb}^{3+}$  ions. On the other hand,  $\text{Tb}^{3+}$  initially increases until it reaches an optimum concentration at 65 mol % and eventually decreases with further addition of  $\text{Tb}^{3+}$  into the host.

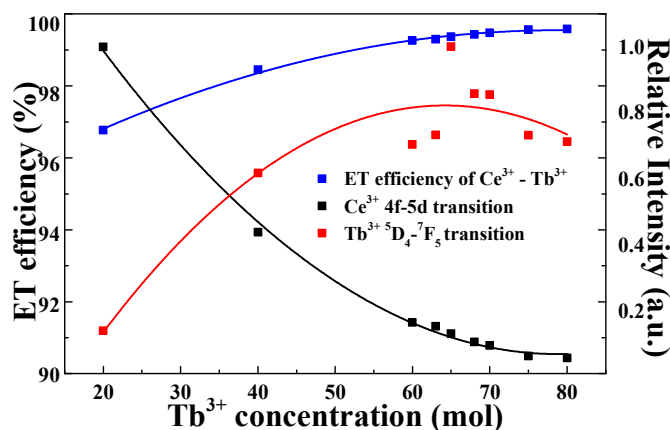


Figure 10. Dependence of  $\text{Ce}^{3+}$  emission (4f  $\rightarrow$  5d),  $\text{Tb}^{3+}$  emission ( $^5\text{D}_4 \rightarrow ^7\text{F}_5$ ) and energy transfer efficiency as a function of  $\text{Tb}^{3+}$ .

Besides from spectral overlap, efficient energy transfer involves strong interactions. It may transpire under radiative transfer through photons which is nearly distance independent and non-radiative transfer which is associated with the resonance between the donor and acceptor. It can be either exchange interaction or multipolar interaction [24-25]. To calculate the critical distance ( $R_c$ ) between  $\text{Ce}^{3+}$  ions and  $\text{Tb}^{3+}$  ions, the following equation is used [9,10,24]:

$$R_c \approx 2 \left[ \frac{3V}{4\pi\chi_c N} \right]^{1/3} \quad (2)$$

where  $V$  is the volume of the unit cell ( $V = 762.43 \text{ \AA}^3$ ),  $\chi_c$  is the total concentration of  $\text{Ce}^{3+}$  and  $\text{Tb}^{3+}$  at maximum intensity ( $\chi_c = 0.68$ ) and  $N$  is the number of host cations in the unit cell ( $N = 4$ ). Using Eq. (2) the calculated critical distance is approximately 8.12  $\text{\AA}$ .  $R_c$  should be less than 5  $\text{\AA}$  in an exchange interaction. Thus, the principle governing the energy transfer is multipolar interaction. [5,24]. According to Dexter's energy transfer formula of multipolar interaction and Reisfeld's approximation, the following relationship is obtained [1,6,8,9,24]:

$$\frac{\eta_0}{\eta} \propto C_{\text{Ce+Tb}}^{n/3} \quad (3)$$

where  $\eta$  and  $\eta_0$  are the luminescence quantum efficiencies of  $\text{Ce}^{3+}$  with and without  $\text{Tb}^{3+}$  ions present, respectively. The ratio  $\eta/\eta_0$  can be estimated by the ratio of relative emission intensities,  $I_{SO}/I_S$  in the absence and presence of activator.  $C_{\text{Ce+Tb}}$  is the total concentration of  $\text{Ce}^{3+}$  and  $\text{Tb}^{3+}$  and  $n = 6, 8$  and  $10$  corresponds to dipole-dipole, dipole-quadrupole and quadrupole-quadrupole mechanisms, respectively [1,6,8,9,24].

In order to further comprehend the energy transfer mechanism between  $\text{Ce}^{3+}$  and  $\text{Tb}^{3+}$  ions, Figures 11 (a), (b) and (c) illustrate the relationships of  $I_{SO}/I_S$  and  $C^{n/3}$ . Among these three, Figure 10 (c) demonstrates the most commendable linear relationship. Therefore, it signifies that the energy transfer mechanism between  $\text{Ce}^{3+}$  and  $\text{Tb}^{3+}$  in  $\text{Li}_6\text{Lu}(\text{BO}_3)_3$  host is governed by quadrupole-quadrupole interaction.

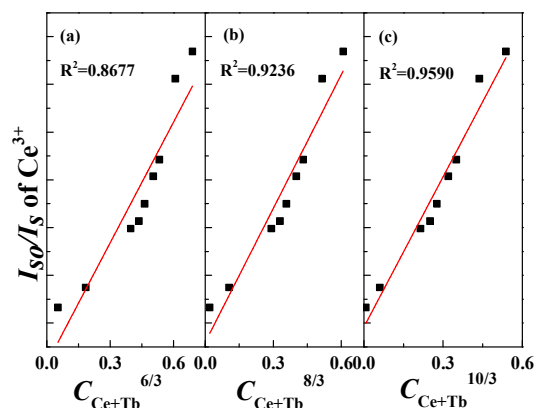


Figure 11. The dependence of  $I_{50}/I_S$  of  $Ce^{3+}$  on (a)  $C_{Ce-Tb}^{6/3}$ , (b)  $C_{Ce-Tb}^{8/3}$  and (c)  $C_{Ce-Tb}^{10/3}$ .

Aside from high luminescence, another crucial property of LED phosphors is thermal stability predominantly for high power LEDs in which the operating temperature can reach up to 450 K [12]. Figure 12 (a) depicts the temperature dependence of the luminescence intensity of  $Li_6Lu(BO_3)_3: 0.03Ce^{3+}, 0.65Tb^{3+}$  excited at 350 nm in the temperature range of 298 K – 573 K. The maximum peak is constantly located at 543 nm even at higher temperature. The emission intensity progressively decreases as the temperature increases due to thermal quenching. Figure 12 (b) presents the normalized intensity of the thermal luminescence. At 373 K, the thermal luminescence is reduced by almost 12%, at 473 K the intensity is decreased to 50% and at 573 K, the thermal luminescence is reduced by approximately 76%.

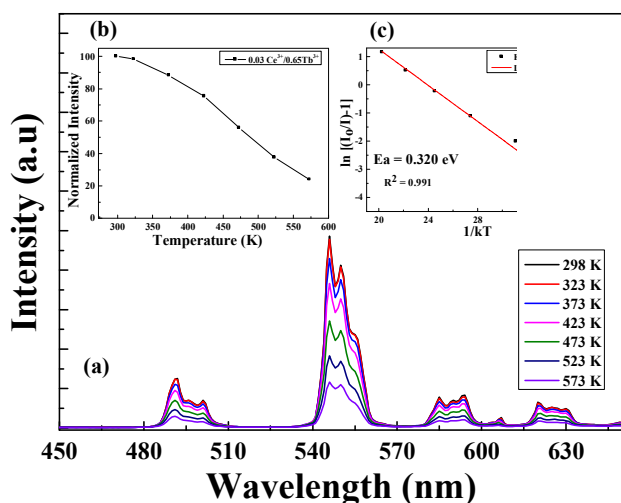


Figure 12. (a) Thermal luminescence of  $Li_6Lu_{0.32}(BO_3)_3: 0.03Ce^{3+}, 0.65Tb^{3+}$  excited at 350 nm. The insets show (b) Normalized intensity as a function of temperature and (c) the graph of  $\ln[(I_0/I)-1]$  versus  $1/\kappa T$ .

To promote better understanding of the relationship between the temperature and luminescence intensity and to determine the activation energy for thermal quenching, the gathered data were fitted to the Arrhenius equation [12,14]:

$$I(T) = \frac{I_0}{1 + A \exp(-\Delta E / \kappa T)} \quad (4)$$

where  $I(T)$  is the intensity at given temperature  $T$ ,  $I_0$  is the initial intensity,  $A$  is a constant,  $\kappa$  is the Boltzmann constant ( $8.617 \times 10^{-5}$  eV  $K^{-1}$ ) and  $E$  is the activation energy for thermal quenching. Figure 12 (c) plots the  $\ln[(I_0/I)-1]$  versus  $1/\kappa T$  and the activation energy is calculated to be 0.320 eV. The high activation energy indicates good thermal stability.

#### CIE Coordinates of $Li_6Lu_{0.97}(BO_3)_3:0.03Ce^{3+}$ and $Li_6Lu_{0.97-y}(BO_3)_3:0.03Ce^{3+}, yTb^{3+}$ phosphors

Commission International de l'Eclairage (CIE) chromaticity coordinates of the samples are presented in Figure 13 and summarized in Table 1. The CIE coordinates illustrate that with increasing  $Tb^{3+}$  concentration, the chromaticity is tuned from blue to green as a result of the cross-relaxation between  $^5D_3$  level and  $^5D_4$  level. Table 1 also shows the relative intensity of  $^5D_4 \rightarrow ^7F_5$  transition and it indicates that the influence of energy transfer between  $Ce^{3+}$  and  $Tb^{3+}$  has significantly improved the luminescence properties of the phosphor. At 350 nm, the relative intensity of  $Li_6Lu(BO_3)_3: 0.03Ce^{3+}, 0.65Tb^{3+}$  was enhanced by 178%. It is also noticeable that  $Li_6Lu_{0.97}(BO_3)_3:0.03Ce^{3+}$  has high color purity.

Table 1. Chromaticity coordinates of  $Li_6Lu_{0.97}(BO_3)_3:0.03Ce^{3+}$  and  $Li_6Lu_{0.97-y}(BO_3)_3:0.03Ce^{3+}, yTb^{3+}$  phosphors.

Phosphors	Excitation Wavelength (nm)	CIE chromaticity coordinates		$^5D_4 \rightarrow ^7F_5$ Relative Intensity
		x	y	
1. $Li_6Lu_{0.97}(BO_3)_3:0.03Ce^{3+}$	350	0.162	0.015	0
2. $Li_6Lu_{0.77}(BO_3)_3:0.03Ce^{3+}, 0.20Tb^{3+}$	350	0.317	0.519	1.00
3. $Li_6Lu_{0.57}(BO_3)_3:0.03Ce^{3+}, 0.40Tb^{3+}$	350	0.334	0.570	1.43
4. $Li_6Lu_{0.37}(BO_3)_3:0.03Ce^{3+}, 0.60Tb^{3+}$	350	0.340	0.586	1.50
5. $Li_6Lu_{0.32}(BO_3)_3:0.03Ce^{3+}, 0.65Tb^{3+}$	350	0.340	0.588	1.78
6. $Li_6Lu_{0.27}(BO_3)_3:0.03Ce^{3+}, 0.70Tb^{3+}$	350	0.342	0.589	1.64
7. $Li_6Lu_{0.22}(BO_3)_3:0.03Ce^{3+}, 0.75Tb^{3+}$	350	0.342	0.593	1.53

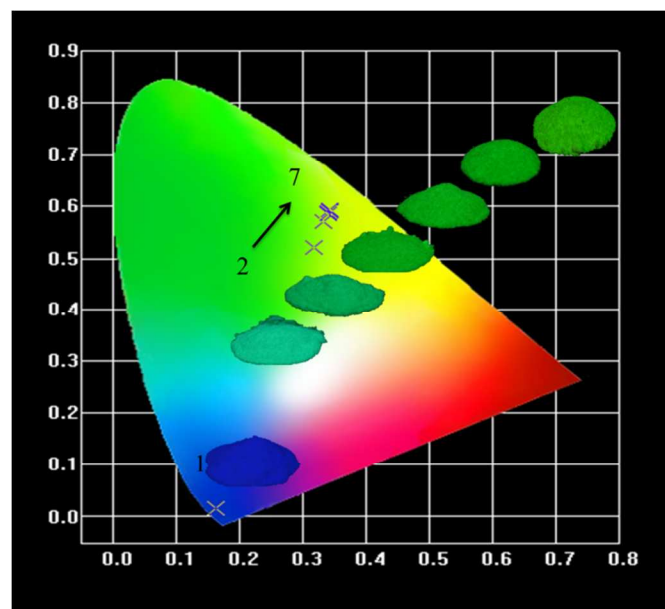


Figure 13. CIE coordinates of  $Li_6Lu_{0.97}(BO_3)_3:0.03Ce^{3+}$  and  $Li_6Lu_{0.97-y}(BO_3)_3:0.03Ce^{3+}, yTb^{3+}$  ( $y = 0.20$  to  $0.75$ ) phosphors under 350 nm excitation.

## Conclusions

A series of tunable blue to green emitting  $Li_6Lu_{0.97-y}(BO_3)_3:0.03Ce^{3+}, yTb^{3+}$  phosphors were successfully synthesized via conventional solid state reaction. Pure phased samples were successfully obtained even at high  $Tb^{3+}$  doping

concentration. The energy absorbed by  $\text{Ce}^{3+}$  ions were efficiently transferred to  $\text{Tb}^{3+}$  since the 5d energy level of  $\text{Ce}^{3+}$  ions is close to the  $^5\text{D}_3$  level of  $\text{Tb}^{3+}$  ions resulting in improved photoluminescence properties of the phosphors. The gathered results indicate that  $\text{Ce}^{3+}$  is an efficient sensitizer for  $\text{Tb}^{3+}$ . The energy transfer is governed by a resonant type quadrupole-quadrupole interaction and the energy transfer critical distance is calculated to be 8.12 Å. The high activation energy denotes high thermal stability of the phosphor. The color of  $\text{Li}_6\text{Lu}(\text{BO}_3)_3:\text{Ce}^{3+},\text{Tb}^{3+}$  phosphor can be modified from blue to green under UV radiation and shows a great potential for W-LED applications.

### Acknowledgments

This research is supported by the National Science Council of Taiwan under contract numbers: 102-2221-E-033-050- MY2 and 102-3011-P-033-003.

### Notes and references

- 1 Y. Jin, Y. Hu, X. Wang, Z. Mu, G. Ju, Z. and Z. Yang, *Physica B*, 2014, **436**, 105-110.
- 2 W.R. Liu, C.H. Huang, C.P. Wu, Y.C. Chiu, Y.T. Yeh and T.M. Chen, *J. Mater. Chem.*, 2011, **21**, 6869-6874.
- 3 C. Guo, X. Ding, H.J. Seo, Z. Ren and J. Bai, *J. Alloys Compd.*, 2011, **509**, 4871-4874.
- 4 P.L. Lin, Z.P. Yang, Z.J. Wang and Q.L. Guo, *Chin. Phys. Lett.*, 2007, **24**, 2977-2979.
- 5 M. Yang, L. Liu and F. Chen, *Mater. Lett.*, 2012, **88**, 116-118.
- 6 X. Fu, L. Fang, S. Niu and H. Zhang, *J. Lumin.*, 2013, **142**, 163-166.
- 7 Y. Zhang, L. Wu, M. Ji, B. Wang, Y. Kong and J. Xu, *Opt. Soc. Am.*, 2011, **2**, 92-102.
- 8 J. Zheng, C. Guo, X. Ding, Z. Ren and J. Bai, *Curr. Appl. Phys.*, 2012, **12**, 643-647.
- 9 J. Sun, Y. Sun, J. Lai, Z. Xia and H. Du, *J. Lumin.*, 2012, **132**, 3048-3052.
- 10 H. Yu, W. Zi, S. Lan, S. Gan, H. Zou, X. Xu and G. Hong, *Opt. Laser Technol.*, 2012, **44**, 2306-2311.
- 11 Q. Wang, D. Deng, Y. Hua, L. Huang, H. Wang, S. Zhao, G. Jia, C. Li and S. Xu, *J. Lumin.*, 2012, **132**, 434-438.
- 12 F. Zhang, Y. Wang and Y. Tao, *J. Lumin.*, 2013, **136**, 51-56.
- 13 L. H. Jiang, Y. L. Zhang, C. Y. Li, R. Pang, J. Q. Hao and Q. Su, *J. Lumin.*, 2008, **128**, 1904-1908.
- 14 H. Lin, H. Liang, Z. Tian, B. Han, J. Wang, Q. Su and G. Zhang, *J. Phys D: Appl. Phys.*, 2009, **42**, 1-9.
- 15 A. A. Reddy, S. Das, A. GOel, R. Sen, R. Siegel, L. Mafra, G. V. Prakash, and J. M. F. Ferreira, *AIP Adv.*, 2013, **3**, 1-15.
- 16 F. Yang, S. K. Pan, D. Z. Ding, X. F. Chen, H. Feng and G. H. Ren, *J. Cryst. Growth*, 2010, **312**, 2411-2414.
- 17 G. Ju, Y. Hu, H. Wu, Z. Yang, C. Fu, Z. Mu and F. Kang, *Opt. Mater.* 2011, **33**, 1297-1301.
- 18 F. Zhang, Y. Wang and Y. Tao, *Phys. Procedia*, 2012, **29**, 55-61.
- 19 H. Nishimura, S. Hosoya, H. Takashima and Y. Kanno, *JPN J. Appl. Phys.*, 2006, **45**, 909-911.
- 20 U. Fawad, M. Oh, H. Park and H. J. Kim, *J. Korean Phys. Soc.*, 2013, **62**, 1102-1107.
- 21 Y. Yang, A. Bao, H. Lai, Y. Tao and H. Yang, *J. Phys. Chem. Solids*, 2009, **70**, 1317-1321.
- 22 U. Manik, S. C. Gedam and S. J. Dhoble, *J. Lumin.*, 2013, **136**, 191-195.
- 23 B. V. Rao, Y. T. Nien, W. S. Hwang and I. G. Chen, *J. Electrochem. Soc.*, 2009, **156**, J338-J341.
- 24 I. V. B. Maggay, P. C. Lin and W. R. Liu, *J. Solid-State Lighting*, 2014, **1**, 1-15.
- 25 G. Ju, Y. Hu, L. Chen, X. Wang, Z. Mu, H. Wu and F. Kang, *J. Electrochem. Soc.*, 2011, **158**, J294-J299.
- 26 J. Sun, J. Lai, J. Zhu, Z. Xia and H. Du, *Ceram. Int.*, 2012, **38**, 5341-5345.
- 27 J. Sun, Z. Lian, G. Shen and D. Shen, *RSC Adv.*, 2013, **40**, 18395-18405.



## Table of Contents Graphic and Summary

Irish Valerie B. Maggay, Pin-Chun Lin and Wei-Ren Liu

*RSC Advances*  
2014, xx, XXXX

Investigation of luminescence properties and energy transfer mechanism of  $\text{Li}_6\text{Lu}(\text{BO}_3)_3$ :  $\text{Ce}^{3+}$ ,  $\text{Tb}^{3+}$  green-emitting phosphors

Novel green-emitting phosphor -  $\text{Li}_6\text{Lu}(\text{BO}_3)_3$ :  $\text{Ce}^{3+}$ ,  $\text{Tb}^{3+}$  phosphors exhibit intense green emission via the energy transfer from  $\text{Ce}^{3+}$  to  $\text{Tb}^{3+}$ . The data demonstrated that the phosphor is a promising green-emitting phosphor for UVLED applications.

